

# Polarization Dependence of Anomalous X-ray Scattering in Orbital Ordered Manganites

Sumio Ishihara and Sadamichi Maekawa

*Institute for Materials Research, Tohoku University, Sendai, 980-8577 Japan*

(February 24, 2018)

In order to determine types of the orbital ordering in manganites, we study theoretically the polarization dependence of the anomalous X-ray scattering which is caused by the anisotropy of the scattering factor. The general formulae of the scattering intensity in the experimental optical system is derived and the atomic scattering factor is calculated in the microscopic electronic model. By using the results, the X-ray scattering intensity in several types of the orbital ordering is numerically calculated as a function of azimuthal and analyzer angles.

71.10.-w, 75.90.+w, 78.70.Ck

## I. INTRODUCTION

Perovskite manganites and their related compounds,  $(R_{1-x}A_x)_{1+n}Mn_nO_{3n+1}$  ( $n = 1, 2, \infty$ , R = rare earth ion, A = alkaline earth ion), have been studied extensively from the fundamental scientific view point as well as the technological one, since the discovery of the colossal magnetoresistance (CMR).<sup>1-4</sup> In order to explain the unique magnetic and transport properties, special attention is paid to the orbital degrees of freedom in Mn ions.<sup>5-11</sup> The electron configuration of a Mn<sup>3+</sup> ion is represented by  $(t_{2g})^3(e_g)^1$  due to the strong Hund coupling. Since an electron occupies the two degenerate  $e_g$  orbitals, the ion has the orbital degrees of freedom as well as spin and charge. It was supposed that the orbital ordering is realized in insulating compounds  $RMnO_3$ <sup>5,6,12,13</sup>,  $R_0.5A_0.5MnO_3$ <sup>5,12,14,15</sup> and  $La_0.5Sr_{1.5}MnO_4$ .<sup>16</sup> Furthermore, in the metallic phase, roles of the orbital degrees in the magnetic, optical and transport phenomena were also stressed.<sup>11,17-19</sup> However, the direct observation of the orbital degrees was restricted experimentally to the case where the polarized neutron diffraction is utilized.<sup>20</sup>

Recently, Murakami *et al.* have applied the anomalous X-ray scattering in order to detect the orbital ordering in single layered manganites  $La_0.5Sr_{1.5}MnO_4$ .<sup>21</sup> They focused on a reflection at  $(\frac{3}{4} \frac{3}{4} 0)$  point and observed a resonant-like peak near the K-edge of a Mn<sup>3+</sup> ion below about 200K. They further observed the unique polarization dependence which is attributed to the tensor character of the anomalous scattering factor. Since all Mn<sup>3+</sup> ions are equivalent, the reflection at  $(\frac{3}{4} \frac{3}{4} 0)$  is forbidden. Therefore, an appearance of the intensity implies that two kinds of orbital are alternately aligned in the MnO<sub>2</sub> plane. This type of the orbital ordering

is termed the antiferro-type orbital ordering, hereafter. The experimental results also imply that the dipole transition between Mn 1s and Mn 4p orbitals causes the scattering. The experimental method was extended to  $La_{1-x}Sr_xMnO_3$  with  $x = 0.0$ <sup>22</sup> and  $0.12$ .<sup>23</sup>

In this paper, we study theoretically the polarization dependence of the anomalous X-ray scattering as a probe to identify types of the orbital ordering in manganites. Although the phenomenological model for the anomalous scattering factor was used to analyze the experimental results of  $(\frac{3}{4} \frac{3}{4} 0)$  reflection, it was not determined which type of the orbital ordering,  $(3d_{3x^2-r^2}, 3d_{3y^2-r^2})$  or  $(3d_{z^2-x^2}, 3d_{y^2-z^2})$ , is realized in  $La_0.5Sr_{1.5}MnO_4$ .<sup>21</sup> As for the theoretical side, several types of the orbital ordering is predicted in the wide range of the carrier concentration.<sup>5,7-11,17,24-28</sup> Once a method to identify types of the orbital ordering is established, this becomes applicable to the study of the orbital structure in not only manganites but also a wide range of transition metal oxides. Considering the fact that types of the orbital ordering directly reflects on the anisotropy of tensor element of the anomalous scattering factor,<sup>29,30</sup> we investigate the polarization dependence of the scattering intensity. Through the numerical calculation in several orbital ordered cases, we propose the method to identify the orderings.

In Sect. II, the general formulae of the polarization dependence of the scattering intensity is derived. In Sect. III, the anomalous part of the atomic structure factor is calculated in a MnO<sub>6</sub> cluster.<sup>31</sup> In Sect IV, the numerical results of the polarization dependence in several orbital ordered cases, which are calculated by using the results obtained in Sects. II and III, are presented. Sect. V is devoted to the summary and discussion.

## II. GENERAL FORMULAE

In this section, we derive the general formulae of the polarization dependence of the scattering intensity in orbital ordered manganites. The conventional experimental arrangement, where the polarization measurement is carried out, is shown in Fig.1.<sup>21,32</sup> It mainly consists of a sample crystal and the polarization analyzer including analyzer crystal and photon detector. The polarization scan is characterized by two rotation angles, i.e., the azimuthal angle ( $\varphi$ ) and the analyzer one ( $\varphi_A$ ). The former is the rotation angle of the sample around the scattering vector  $\vec{K} = \vec{k}'' - \vec{k}'$ , and the latter is that of the analyzer

around an axis which is parallel to the scattered photon beam. The incident beam from the synchrotron source is almost perfectly polarized in the horizontal plane, i.e.,  $\sigma$ -polarization. The direction of the electric vector of the incident photon with respect to the crystalline axis is changed by the azimuthal rotation. The scattered photon has both  $\pi$ - and  $\sigma$ -polarization components, due to the tensor character of the anomalous scattering factor, which are separated by the analyzer scan.

In this optical system, the scattering intensity is given by<sup>32,33</sup>

$$I(\vec{k}', \vec{k}'', \varphi, \varphi_A) = \sum_{\lambda'} \left| \sum_{\lambda} M_{\lambda' \lambda}(\varphi_A) A_{\lambda \sigma}(\vec{k}', \vec{k}'', \varphi) \right|^2, \quad (1)$$

for  $\lambda(\lambda') = \sigma$  or  $\pi$ .  $M_{\lambda' \lambda}(\varphi_A)$  is the scattering matrix in the analyzer and described by the analyzer angle and the scattering one  $\theta_A$  in the analyzer as follows,

$$M_{\lambda' \lambda}(\varphi_A) = F_A \begin{pmatrix} \cos \varphi_A & -\sin \varphi_A \\ \sin \varphi_A \cos 2\theta_A & \cos \varphi_A \cos 2\theta_A \end{pmatrix}, \quad (2)$$

where  $F_A$  is the scattering factor in the analyzer crystal. In this paper, the scattering angle is fixed at  $\theta_A = \pi/4$ , as chosen in the conventional experiments. The  $\sigma$ - and  $\pi$ -polarized components in the scattered photon are detected by the photon detector with  $\varphi_A = 0$  and  $\pi/2$ , respectively.  $A_{\lambda'' \lambda'}(\vec{k}'', \vec{k}', \varphi)$  in Eq. (1) is the scattering amplitude with the incident (scattered) photon momentum  $\vec{k}'$  ( $\vec{k}''$ ) and the polarization  $\lambda'$  ( $\lambda''$ ) as a function of the azimuthal angle. It is given by,

$$A_{\lambda'' \lambda'}(\vec{k}'', \vec{k}', \varphi) = \frac{e^2}{mc^2} \sum_{\alpha'' \alpha'} \epsilon_{\lambda'' \alpha''}^{(s)} \times \left[ U(\varphi) V F(\vec{k}', \vec{k}'') V^\dagger U(\varphi)^\dagger \right]_{\alpha'' \alpha'} \epsilon_{\lambda' \alpha'}^{(i)t}, \quad (3)$$

where  $F_{\alpha \beta}(\vec{k}', \vec{k}'')$  is the structure factor of the sample crystal defined in the coordinate of the crystallographic axis described as  $(\hat{a}, \hat{b}, \hat{c})$ .  $\epsilon_{\lambda \alpha}^{(i)}$  and  $\epsilon_{\lambda \alpha}^{(s)}$  are the polarization vectors of the incident and scattered photons, respectively, and their explicit forms are given by

$$\epsilon_{\lambda \alpha}^{(i)} = \begin{pmatrix} 1 & 0 & 0 \\ 0 & \sin \theta & \cos \theta \end{pmatrix}, \quad (4)$$

and

$$\epsilon_{\lambda \alpha}^{(s)} = \begin{pmatrix} 1 & 0 & 0 \\ 0 & -\sin \theta & \cos \theta \end{pmatrix}, \quad (5)$$

where the suffix  $\alpha$  denotes the Cartesian coordinate in the laboratory system, i.e.,  $(\hat{e}_1, \hat{e}_2, \hat{e}_3)$  shown in Fig. 1.  $\epsilon_{\lambda \alpha}^{(i)t}$  is the transposed matrix of  $\epsilon_{\lambda \alpha}^{(i)}$ . The unitary matrix  $U(\varphi)$  in Eq. (3) describes the azimuthal rotation of the sample around the  $\hat{e}_3$ -axis defined by

$$U(\varphi) = \begin{pmatrix} \cos \varphi & -\sin \varphi & 0 \\ \sin \varphi & \cos \varphi & 0 \\ 0 & 0 & 1 \end{pmatrix}, \quad (6)$$

and the unitary matrix  $V$  describes the transformation from the coordinate in the crystallographic axis  $(\hat{a}, \hat{b}, \hat{c})$  to that in the laboratory system  $(\hat{e}_1, \hat{e}_2, \hat{e}_3)$ . The structure factor  $F_{\alpha \beta}(\vec{k}', \vec{k}'')$  in Eq.(3) is represented by a sum of the normal and anomalous parts of the scattering factor as follows:

$$F_{\alpha \beta}(\vec{k}', \vec{k}'') = N \sum_{i \in \text{cell}} e^{i(\vec{k}' - \vec{k}'') \cdot \vec{r}_i} f_{i \alpha \beta}(\vec{k}', \vec{k}''), \quad (7)$$

with

$$f_{i \alpha \beta}(\vec{k}', \vec{k}'') = f_{0i}(\vec{k}', \vec{k}'') \delta_{\alpha \beta} + \Delta f_{i \alpha \beta}(\vec{k}', \vec{k}''). \quad (8)$$

Here,  $f_{0i}(\vec{k}', \vec{k}'')$  and  $\Delta f_{i \alpha \beta}(\vec{k}', \vec{k}'')$  are the normal and anomalous parts of the atomic scattering factor, respectively, of the  $i$ -th atom defined in the  $(\hat{a}, \hat{b}, \hat{c})$ -coordinate.  $N$  is the number of the unit cell. When we determine the unitary matrix  $V$  and the atomic scattering factors, the scattering intensity is calculated as a function of the azimuthal angle  $\varphi$  and the analyzer angle  $\varphi_A$ .

It is instructive to demonstrate the polarization dependence of the scattering intensity in the following two cases: (i)  $(\hat{e}_1, \hat{e}_2, \hat{e}_3) = (\hat{a}, \hat{b}, \hat{c})$  (azimuthal rotation around the  $c$ -axis) and (ii)  $(\hat{e}_1, \hat{e}_2, \hat{e}_3) = (\hat{c}, \frac{1}{\sqrt{2}}(\hat{a} - \hat{b}), \frac{1}{\sqrt{2}}(\hat{a} + \hat{b}))$  (azimuthal rotation around the  $\hat{a} + \hat{b}$ -axis). When the crystallographic axes coincide with the principle ones in the  $\text{MnO}_6$  octahedron, the anomalous part of the scattering factor in Eq. (8) is diagonal as  $\Delta f_{i \alpha \beta}(\vec{k}', \vec{k}'') = \delta_{\alpha \beta} \Delta f_{i \alpha \alpha}(\vec{k}', \vec{k}'')$ . In this condition, the scattering intensity is given by

$$I(\vec{k}', \vec{k}'', \varphi, \varphi_A) = \left( \frac{e^2}{mc^2} \right)^2 |F_A|^2 \times |D_{\sigma \sigma} \cos \varphi_A - D_{\pi \sigma} \sin \varphi_A|^2, \quad (9)$$

with

$$D_{\sigma \sigma} = F_{xx} \cos^2 \varphi + F_{yy} \sin^2 \varphi, \quad (10)$$

and

$$D_{\pi \sigma} = (-F_{xx} + F_{yy}) \sin \varphi \cos \varphi \sin \theta, \quad (11)$$

for case (i), and

$$D_{\sigma \sigma} = F_{zz} \cos^2 \varphi + \frac{1}{2}(F_{xx} + F_{yy}) \sin^2 \varphi, \quad (12)$$

and

$$D_{\pi \sigma} = \frac{1}{2}(F_{xx} + F_{yy} - 2F_{zz}) \sin \varphi \cos \varphi \sin \theta + \frac{1}{2}(-F_{xx} + F_{yy}) \sin \varphi \cos \theta, \quad (13)$$

for case (ii).

### III. ATOMIC SCATTERING FACTOR

The normal and anomalous parts of the atomic scattering factor in Eq.(8) are obtained by the perturbation calculation with respect to the electron-photon interaction. The normal part is given by the Fourier transform of the charge density  $\rho_i$  in the  $i$ -th atom defined by  $f_{0i} = \langle f | \rho_i(\vec{K} = \vec{k}'' - \vec{k}') | 0 \rangle$ , where  $|0\rangle$  ( $|f\rangle$ ) is the initial (final) electronic state with energy  $\varepsilon_0$  ( $\varepsilon_f$ ). The anomalous one is derived by the interaction between electronic current and photon and is expressed as follows:<sup>34,35</sup>

$$\Delta f_{i\alpha\beta}(k', k'') = \frac{m}{e^2} \sum_l \left\{ \frac{\langle f | j_{i\alpha}(-\vec{k}') | l \rangle \langle l | j_{i\beta}(k'') | 0 \rangle}{\varepsilon_0 - \varepsilon_l - \omega_{k''} - i\delta} + \frac{\langle f | j_{i\beta}(\vec{k}'') | l \rangle \langle l | j_{i\alpha}(-\vec{k}') | 0 \rangle}{\varepsilon_0 - \varepsilon_l + \omega_{k'} - i\delta} \right\}, \quad (14)$$

where  $|l\rangle$  is the intermediate electronic state with energy  $\varepsilon_l$  and  $\delta$  is a damping constant. The current operator  $j_{i\alpha}(\vec{k}) = \frac{e}{m} \sum_\sigma (A_\alpha(\vec{k}) P_{i\alpha\sigma}^\dagger s_{i\sigma} + h.c.)$  describes the dipole transition between Mn 1s and 4p orbitals. Here,  $P_{i\alpha\sigma}$  and  $s_{i\sigma}$  are the annihilation operators of electron in Mn 4p and Mn 1s orbitals, respectively, with spin  $\sigma$  and Cartesian coordinate  $\alpha$ .  $A_\alpha(\vec{k})$  is the coupling constant between the current and the photon. The contribution from the quadrupole transition is small, because the inversion symmetry is preserved in this system.<sup>36</sup> As shown in the next section, the anisotropy of the tensor element in the anomalous scattering factor determines the polarization dependence of the scattering intensity.

The anomalous part of the atomic scattering factor  $\Delta f_{i\alpha\beta}(k', k'')$  is calculated in the microscopic electronic model. We consider a MnO<sub>6</sub> octahedron and introduce the following orbitals in a Mn ion: {1s, 3d <sub>$\gamma$</sub>  ( $\gamma = \gamma_{\theta+}, \gamma_{\theta-}$ ), 4p <sub>$\gamma$</sub>  ( $\gamma = x, y, z$ )}, where  $|3d_{\gamma_{\theta+}}\rangle = \cos(\theta^{(t)})/2 |3d_{3z^2-r^2}\rangle + \sin(\theta^{(t)})/2 |3d_{x^2-y^2}\rangle$  and  $|3d_{\gamma_{\theta-}}\rangle = -\sin(\theta^{(t)})/2 |3d_{3z^2-r^2}\rangle + \cos(\theta^{(t)})/2 |3d_{x^2-y^2}\rangle$ . Six O 2p orbitals, which contribute to the  $\sigma$ -bond with the Mn 3d orbitals, are also considered. These are denoted as 2p <sub>$i$</sub>  ( $i = 1 \sim 6$ ) where 2p<sub>1(2)</sub>, 2p<sub>3(4)</sub> and 2p<sub>5(6)</sub> are 2p <sub>$x$</sub>  orbital at the position of  $(+(-)a/2, 0, 0)$ , 2p <sub>$y$</sub>  at  $(0, +(-)a/2, 0)$ , and 2p <sub>$z$</sub>  at  $(0, 0, +(-)a/2)$ , respectively, with Mn-O bond length  $a/2$ . The position of the Mn ion is chosen to be  $(0, 0, 0)$ . By utilizing the irreducible representation in  $O_h$  group, these O 2p orbitals are recombined as {2p <sub>$\gamma_{\theta+}$</sub> , 2p <sub>$\gamma_{\theta-}$</sub> , 2p <sub>$x$</sub> , 2p <sub>$y$</sub> , 2p <sub>$z$</sub> , 2p <sub>$r^2$</sub> }. For example, 2p<sub>3z<sup>2</sup>-r<sup>2</sup></sub> and 2p <sub>$x$</sub>  orbitals are represented as  $2p_{3z^2-r^2} = \frac{1}{\sqrt{3}}(\frac{1}{2}(-2p_1 + 2p_2 - 2p_3 + 2p_4) + 2p_5 - 2p_6)$ , and  $2p_x = \frac{1}{\sqrt{2}}(2p_1 + 2p_2)$ .

On these bases, we set up the following Hamiltonian:

$$H = H_0 + H_t + H_{3d-4p} + H_{4p-2p} + H_{core} + H_{3d-3d}. \quad (15)$$

The first and second terms describe the energy level in each orbital and the electron transfer between Mn 3d and O 2p orbitals, respectively, and are given by

$$\begin{aligned} H_0 + H_t = & \sum_{\gamma\theta\sigma} \varepsilon_d d_{\gamma\theta\sigma}^\dagger d_{\gamma\theta\sigma} + \sum_{\gamma\sigma} \varepsilon_P P_{\gamma\sigma}^\dagger P_{\gamma\sigma} \\ & + \sum_{\Gamma=\gamma, \gamma\theta} \varepsilon_p p_{\Gamma\sigma}^\dagger p_{\Gamma\sigma} + \sum_{\sigma} \varepsilon_s s_{\sigma}^\dagger s_{\sigma} \\ & + \sqrt{3} t_{3d-2p} \sum_{\gamma\theta\sigma} \left( d_{\gamma\theta\sigma}^\dagger p_{\gamma\theta\sigma} + h.c. \right), \end{aligned} \quad (16)$$

where,  $d_{\gamma\theta\sigma}$ , and  $p_{\Gamma\sigma}$  are the electron annihilation operators in Mn 3d, and O 2p orbitals, respectively, with spin  $\sigma$  and orbital  $\gamma\theta$  ( $= \gamma_{\theta+}, \gamma_{\theta-}$ ) and  $\gamma$  ( $= x, y, z$ ). The third and fourth terms in Eq.(15), which describe the Coulomb interaction between Mn 3d and Mn 4p orbitals and Mn 4p and O 2p orbitals, respectively, are given by

$$\begin{aligned} H_{3d-4p} + H_{4p-2p} = & \sum_{\gamma\theta\gamma} V(3d_{\gamma\theta}, 4p_\gamma) n(3d_{\gamma\theta}) n(4p_\gamma) \\ & + \sum_{\gamma\theta\gamma} V(4p_\gamma, 2p_{\gamma\theta}) n(4p_\gamma) n_h(2p_{\gamma\theta}). \end{aligned} \quad (17)$$

$n(3d_{\gamma\theta})$  and  $n(4p_\gamma)$  are the number operators of Mn 3d and Mn 4p electrons, respectively, and  $n_h(2p_\gamma)$  is the number operator of the O 2p holes. The explicit forms of the Coulomb interaction in Eq.(17) are written by

$$\begin{aligned} V(3d_{\gamma\theta\pm}, 4p_\gamma) = & F_0(3d, 4p) \\ & \pm 4F_2(3d, 4p) \cos\left(\theta^{(t)} + m_\gamma \frac{2\pi}{3}\right), \end{aligned} \quad (18)$$

and

$$V(2p_{\gamma\theta\pm}, 4p_\gamma) = -\varepsilon \pm \frac{\varepsilon\rho^2}{5} \cos\left(\theta^{(t)} + m_\gamma \frac{2\pi}{3}\right). \quad (19)$$

$m_x = +1$ ,  $m_y = -1$ , and  $m_z = 0$ .  $F_n(3d, 4p)$  is the Slater-integral between 3d and 4p electrons, and is defined by  $F_0(3d, 4p) = F^{(0)}(3d, 4p)$  and  $F_2(3d, 4p) = \frac{1}{35}F^{(2)}(3d, 4p)$ .  $\varepsilon = Ze^2/a$  and  $\rho = \langle r_{4p} \rangle/a$  where  $Z = 2$ , and  $\langle r_{4p} \rangle$  is the average radius of Mn 4p orbital. Furthermore, we introduce the interaction between Mn 3d(4p) electron and Mn 1s core hole as follows;

$$\begin{aligned} H_{core} = & \sum_{\gamma\theta\sigma\sigma'} V(1s, 3d) n(3d_{\gamma\theta\sigma}) n(1s_{\sigma'}) \\ & + \sum_{\gamma\sigma\sigma'} V(1s, 4p) n(4p_{\gamma\sigma}) n(1s_{\sigma'}), \end{aligned} \quad (20)$$

where both  $V(1s, 3d)$  and  $V(1s, 4p)$  do not depend on the orbitals. The last term in Eq.(15),  $H_{3d-3d}$ , is the interaction between Mn 3d electrons<sup>10</sup> defined by

$$\begin{aligned} H_{3d-3d} = & U \sum_{\gamma\theta} n(3d_{\gamma\theta\uparrow}) n(3d_{\gamma\theta\downarrow}) \\ & + U' n(3d_{\gamma\theta+}) n(3d_{\gamma\theta-}) \end{aligned} \quad (21)$$

$$\begin{aligned} & + K \sum_{\sigma\sigma'} d_{\gamma\theta+\sigma}^\dagger d_{\gamma\theta-\sigma'}^\dagger d_{\gamma\theta+\sigma'} d_{\gamma\theta-\sigma} \\ & - J_H \sum_{\gamma\theta} \vec{S}_{t_{2g}} \cdot \vec{s}_{\gamma\theta}, \end{aligned} \quad (22)$$

where  $U$ ,  $U'$  and  $K$  are the Coulomb and exchange interactions between  $3d$  electrons with  $K = (U - U')/2$ .  $J_H$  describes the Hund coupling between the localized  $t_{2g}$  spin ( $\vec{S}_{t_{2g}}$ ) with  $S = 3/2$  and  $e_g$  spin defined by  $\vec{s}_{\gamma\theta} = \frac{1}{2} \sum_{\sigma'\sigma''} d_{\gamma\theta\sigma'}^\dagger(\vec{\sigma})\sigma'\sigma''d_{\gamma\theta\sigma''}$ . The electron transfer ( $t_{4p-2p}$ ) between Mn  $4p$  and O  $2p$  is not included in the model. As mentioned above, the O  $2p$  orbitals are recombined by utilizing the irreducible representation in  $O_h$  group, and the Mn  $3d$  and Mn  $4p$  orbitals are decoupled when  $t_{3d-2p}$  and  $t_{4p-2p}$  are taken into account. Therefore, the essential conclusion about the anisotropy of the atomic scattering factor being based on the Coulomb interactions is not changed, although a large overlap between Mn  $4p$  and O  $2p$  orbitals may reduce the Coulomb interaction between Mn  $3d$  and Mn  $4p$  and increase the one between Mn  $4p$  and O  $2p$ .

It is worth noting that  $H_{3d-4p}$  and  $H_{4p-2p}$  provide the anisotropy of the atomic scattering factor in orbital ordered states. The essential points in the mechanism of the anisotropy is the fact that these interactions depend on the occupied Mn  $3d$  orbitals. When an electron occupies  $3d_{3z^2-r^2}$  orbital ( $\theta^{(t)} = 0$ ), the energy of  $4p_z$  orbital is higher than that of  $4p_{x(y)}$  orbital by  $6F_2(3d, 4p)$  due to  $V(3d_{\gamma\theta}, 4p_{\gamma})$ , as a result, the scattering intensity near the K-edge is dominated by  $4p_{x(y)}$  orbital. Furthermore,  $|3d_{3z^2-r^2}^1\rangle$  state is strongly mixed with  $|3d_{3z^2-r^2}^1 3d_{x^2-y^2}^1 p_{x^2-y^2}^1\rangle$ , where  $|p_{x^2-y^2}\rangle$  describes the state where a hole occupies the O  $2p_{x^2-y^2}$  orbital. Through the inter-atomic Coulomb interaction  $V(2p_{\gamma\theta}, 4p_{\gamma})$ , the energy of  $4p_z$  orbital becomes higher than that of  $4p_{x(y)}$  orbital by  $\frac{3}{10}\varepsilon\rho$ . Therefore, the two interactions due to the intra- and inter-site Coulomb interactions result cooperatively in the anisotropy of the scattering factor. In the following numerical calculation,  $H_{4p-2p}$  is often neglected, since the inter-site interaction is well screened in comparison with the intra-site Coulomb interaction.

The lattice distortion in the  $\text{MnO}_6$  octahedron also becomes the origin of the anisotropy of the scattering factor. When there is the Jahn-Teller(JT)-type lattice distortion characterized by the difference of the bond lengths in the  $ab$ -plane and the  $c$ -direction, i.e.,  $\delta a = a_z - a_{x(y)}$ , the energy difference of the Mn  $4p_{x(y)}$  and  $4p_z$  is brought about. In the case of  $a_z > a_{x(y)}$ , the energy of the Mn  $4p_z$  orbital is relatively stabilized in comparison with that of Mn  $4p_{x(y)}$  orbital. Therefore, this contribution competes with the above originated from the intra- and inter-atomic Coulomb interactions. In  $\text{LaMnO}_3$  where the  $\delta a/a$  is about 15%,<sup>37</sup> the contributions from the Coulomb interactions seems to be weakened by that from the lattice distortion. However, the notable lattice distortion in  $\text{MnO}_6$  octahedron is not observed in  $\text{La}_{0.5}\text{Sr}_{1.5}\text{MnO}_4$ .<sup>38</sup> Furthermore, it was recently reported that in  $\text{La}_{0.88}\text{Sr}_{0.12}\text{MnO}_3$  the X-ray scattering intensity attributed to the anomalous scattering is observed at (030) reflection in the  $O^*$  phase,<sup>23</sup> where the six Mn-O bonds in the  $\text{MnO}_6$  octahedron are equivalent.<sup>37</sup> There-

fore, we conclude that the Coulomb interactions dominate the origin of the anisotropy of the anomalous scattering factor in these compounds and do not introduce the contribution from the lattice distortion in the Hamiltonian in Eq.(15).

By adopting the above Hamiltonian, we calculate the atomic scattering factor in the configuration interaction method.  $|3d_{\gamma\theta+}^1\rangle$  and  $|3d_{\gamma\theta+}^1 3d_{\gamma\theta-}^1 2p_{\gamma\theta-}\rangle$  states are introduced as the bases of the initial and final states, and  $|3d_{\gamma\theta+}^1 4p_{\gamma}^1 1s\rangle$  and  $|3d_{\gamma\theta+}^1 3d_{\gamma\theta-}^1 2p_{\gamma\theta-} 4p_{\gamma}^1 1s\rangle$  states are as the bases of the intermediate states. The second term in the right hand side in Eq. (14) is only considered. The parameter values in the Hamiltonian are chosen to be  $\varepsilon_P - \varepsilon_d = 13.0\text{eV}$ ,  $\varepsilon_p - \varepsilon_d = 2.5\text{eV}$ ,  $t_{3d-2p} = 1.2\text{eV}$ ,  $V(3d, 1s) = V(4p, 1s) = 7.0\text{eV}$ ,  $U = 8.5\text{eV}$ ,  $U' = 6.5\text{eV}$  and  $J_H = 1.0\text{eV}$ . The Slater-integrals between Mn  $4p$  and Mn  $3d$  electrons are chosen to be  $F_0(3d, 4p) = 5.0\text{eV}$  and  $F_2(3d, 4p) = 0.3\text{eV}$  which are the same order as ones between Mn  $3d$  electrons  $F_n(3d, 3d)$  evaluated by the photoemission experiments.<sup>39</sup> The damping parameter  $\delta$  in Eq. (14) is taken to be  $0.5\text{eV}$ .

In Fig. 2, we present the energy dependence of the real and imaginary parts of the anomalous scattering factor. The edge of the lowest peak of  $\Delta f''_{i\alpha\alpha}$  corresponds to the Mn K-edge. Near the edge in Fig. 2(a), where  $3d_{3z^2-r^2}$  orbital is occupied, the anisotropy is clearly shown. The energy position of  $\Delta f''_{ixx}(yy)$  is lower and its weight is larger than those of  $\Delta f''_{izz}$ . In Fig. 2(b) where  $3d_{x^2-y^2}$  orbital is occupied, the anisotropy in the main peak is entirely opposite to that in Fig. 2(a). In both Figs. 2 (a) and (b), the spectra of  $\Delta f_{ixx}$  and  $\Delta f_{iyy}$  are identical as expected.

#### IV. POLARIZATION DEPENDENCE OF THE SCATTERING INTENSITY

By using the general formulae of the scattering intensity (Eq.(1)-(8)) and the atomic scattering factor calculated in the microscopic electronic structure, we numerically calculate the polarization dependence of the normalized scattering intensity  $\tilde{I}(\varphi, \varphi_A) = I(\varphi, \varphi_A)/(N_A^2 e^4/(mc^2)^2 |F_A|^2)$ , where  $N_A$  is the number of the Mn atom. The energy of the incident photon beam is fixed at that of the K-edge in a  $\text{Mn}^{3+}$  ion. In our model, it is chosen to be the energy at which the lowest component of  $\Delta f''_{i\alpha\alpha}$  ( $\alpha = x, y, z$ ) has a half value of its maximum. The normal part of the scattering factor of a  $\text{Mn}^{3+}$  ion is chosen as  $f_{0i}m/|A_{\alpha\alpha}|^2 = 5\text{eV}^{-1}$  which is about 5 times larger than the typical value of  $|\Delta f_{i\alpha\alpha}|m/|A_{\alpha\alpha}|^2$  at the edge.<sup>21</sup> The following part in this section is divided into three subsections and the numerical results calculated in several orbital ordered cases are presented. The qualitative features in the following numerical results, e.g. periodicity and phase of the oscillations as a function of  $\varphi$ , are independent of details of the microscopic calculation shown in the previous section and are

related to symmetry of the orbital ordering and the experimental arrangement, although the detail quantitative ones depend on the adopted interactions and parameter values in the microscopic model.

### A. ferro-type orbital ordering in the simple cubic lattice

We consider the ferro-type orbital ordering (orbital-F) in the simple cubic lattice where a kind of orbital is occupied in each Mn site and demonstrate how to identify types of orbital through the polarization analyses. The numerical results shown in this subsection will help us to understand the polarization dependence of the fundamental reflections in the antiferro-type orbital ordering shown in the next subsection.

In orbital-F case, the structure factor per unit cell (Eq. (7)) is given by  $\frac{1}{N}F_{\alpha\beta} = f_{A\alpha\beta}$  at the  $(hkl) = (n_x n_y n_z)$  reflection with integer  $n_i (i = x, y, z)$ . Here,  $(hkl)$  is the indices in the cubic coordinate defined as  $\vec{K} = h\frac{2\pi}{a}\hat{a} + k\frac{2\pi}{a}\hat{b} + l\frac{2\pi}{a}\hat{c}$  where  $a$  is the lattice parameter in the cubic cell.  $f_{A\alpha\beta}$  is the sum of the normal and anomalous parts in a  $Mn^{3+}$  ion with orbital  $A$ ;  $\delta_{\alpha\beta}f_{0A} + \Delta f_{A\alpha\beta}$ . In Fig. 3(a), we present the scattering intensity with  $\theta_A^{(t)} = 0$  which means that an electron occupies the  $3d_{3z^2-r^2}$  orbital in each  $Mn^{3+}$  ion. It is calculated in the cases of  $(\hat{e}_1, \hat{e}_2, \hat{e}_3) = (\hat{b}, \hat{c}, \hat{a})$  (azimuthal scan around  $a$ -axis). In the case of  $(\hat{e}_1, \hat{e}_2, \hat{e}_3) = (\hat{c}, \hat{a}, \hat{b})$  (azimuthal scan around  $b$ -axis),  $\varphi$  dependence is entirely opposite to that in Fig. 3(a). On the contrary, the intensity is independent of  $\varphi$  in the case where the azimuthal scan is performed around  $c$ -axis. We first consider the contribution from the normal part of the scattering factor. The polarization dependence of the intensity is represented by  $\tilde{I}(\varphi, \varphi_A) = |f_{0A} \cos \varphi_A|^2$ , which is independent of  $\varphi$  due to the scalar character of  $f_{0A}$ . For convenience, the value of  $\varphi_A = 0$  is defined  $I_0 = |f_{0A}|^2$ . This  $\varphi_A$  dependence is interpreted that the scattering at  $\varphi_A = 0 (\pi/2)$  is accompanied with the polarization of  $(\lambda', \lambda'') = (\sigma, \sigma)((\sigma, \pi))$ , where  $\lambda'(\lambda'')$  describes the polarization of the incident(scattered) photon. Therefore, the polarization dependence in Fig. 3(a) is dominated by the normal part of the scattering factor and slightly modified by the anomalous part.

Let us examine the scattering intensity at  $\varphi_A = 0$  in Fig. 3(a). This is represented by

$$\tilde{I}(\varphi, \varphi_A = 0) = |f_{0A} + \Delta f|^2, \quad (23)$$

with

$$\Delta f = \Delta f_{Ayy} \cos^2 \varphi + \Delta f_{Azz} \sin^2 \varphi. \quad (24)$$

Since the normal part of the scattering factor dominates the scattering intensity, it is approximated as  $\tilde{I}(\varphi, \varphi_A = 0) \sim f_{0A}^2 + 2f_{0A}\Delta f_A'$ , where  $\Delta f_A'$  is negative at the

edge. As a result, the real part of the anomalous component decreases the scattering intensity from  $I_0$ . In the case where  $3d_{3z^2-r^2}$  orbital is occupied,  $|\Delta f'_{Axx(yy)}|$  has a larger value at the edge in comparison with  $|\Delta f'_{Azz}|$  (see Figs. 2(a) and (c)). Therefore, the reduction of the scattering intensity from  $I_0$  is remarkable around  $\varphi = 0$  and  $\pi$ , where the electric vector in the incident photon is parallel to the  $b$ -axis.

In Fig. 3(b), we present the polarization dependence of the scattering intensity in several orbital-F cases at  $\varphi_A = 0$ . With increasing  $\theta_A^{(t)}$  from  $\theta_A^{(t)} = 0$ , the  $\varphi$  dependence becomes weak and disappears at  $\theta_A^{(t)} = 2\pi/6$  ( $3d_{y^2-z^2}$ ). With further increasing  $\theta_A^{(t)}$ , the phase of a modulation becomes inverse, since  $\Delta f_{Azz}$  dominates the scattering factor near the edge. The inversion of a modulation in  $\tilde{I}(\varphi, \varphi_A = 0)$  occurs at  $\theta_A^{(t)} = 4\pi/6$  and 0 in the cases of  $(\hat{e}_1, \hat{e}_2, \hat{e}_3) = (\hat{c}, \hat{a}, \hat{b})$  and  $(\hat{a}, \hat{b}, \hat{c})$ , respectively. By combining the azimuthal scan around  $a$ -,  $b$ - and  $c$ -axes, it is possible to identify the occupied orbital in the orbital-F case.

### B. antiferro-type orbital ordering in the simple cubic lattice

Next, we consider the antiferro-type orbital ordering (orbital-AF), where two kinds of orbital sublattice, denoted by  $A$  and  $B$ , exist. In the simple cubic lattice, there are three kinds of orbital-AF, that is, layer-type (orbital-AAF), rod-type (orbital-CAF) and NaCl-type (orbital-GAF). These notations are defined by analogy with types of antiferromagnetic structures.<sup>17,24</sup> In each case, two kinds of the reflection point exist, termed the fundamental reflection at  $(hkl) = (n_x n_y n_z)$  and the orbital superlattice reflection at  $(hkl) = (n_x n_y n_z + \frac{1}{2})$  for orbital-CAF,  $(n_x + \frac{1}{2} n_y + \frac{1}{2} n_z)$  for orbital-AAF and  $(n_x + \frac{1}{2} n_y + \frac{1}{2} n_z + \frac{1}{2})$  for orbital-GAF. By examining the superlattice reflection, the above three types of the orbital-AF is able to be distinguished. The structure factor per unit cell is written as  $\frac{1}{N}F_{\alpha\beta} = (f_{A\alpha\beta} + f_{B\alpha\beta})$  for the fundamental reflection and  $\frac{1}{N}F_{\alpha\beta} = (f_{A\alpha\beta} - f_{B\alpha\beta})$  for the superlattice reflection. For convenience, we define  $f_{+\alpha\beta} = \frac{1}{2}(f_{A\alpha\beta} + f_{B\alpha\beta})$  and  $f_{-\alpha\beta} = \frac{1}{2}(f_{A\alpha\beta} - f_{B\alpha\beta})$ , and term the former and latter the ferro- and antiferro-components of the scattering factor, respectively. We neglect the difference of the normal part of the scattering factors of  $Mn^{3+}$  ions between the  $A$  and  $B$  sublattices. Therefore, at the orbital superlattice reflection, only the antiferro-component of the anomalous part contributes.

In Fig. 4(a), the polarization dependence of the fundamental reflection in the orbital-AF case is presented. The orbital state in the two sublattices is  $(\theta_A^{(t)}, \theta_B^{(t)}) = (4\pi/6, -4\pi/6)$  which corresponds to the  $(3d_{3y^2-r^2}, 3d_{3x^2-r^2})$ -type orbital ordering. The coordinate in the laboratory system is chosen to be  $(\hat{e}_1, \hat{e}_2, \hat{e}_3) = (\hat{b}, \hat{c}, \hat{a})$ . The explicit formula of the intensity in Fig. 4(a)

at  $\varphi_A = 0$  is given by Eq. (23) with

$$\Delta f = \Delta f_{+yy} \cos^2 \varphi + \Delta f_{+zz} \sin^2 \varphi. \quad (25)$$

We note that  $\Delta f_{Ayy}$  and  $\Delta f_{Azz}$  in Eq.(24) are replaced by the ferro-components of the scattering factor, i.e.,  $\Delta f_{+yy}$  and  $\Delta f_{+zz}$  in Eq.(25), respectively. The reduction of the intensity from  $I_0$  becomes remarkable around  $\varphi = \pi/2$  and  $3\pi/2$  where the electric vector in the incident beam is parallel to the  $c$ -axis. This is because the ferro-component of the scattering factor  $\frac{1}{2}(\Delta f_{A\alpha\alpha} + \Delta f_{B\alpha\alpha})$  is larger for  $\alpha = z$  in comparison with that for  $\alpha = x(y)$ , since the  $3d_{3y^2-r^2}$  and  $3d_{3x^2-r^2}$  orbitals are almost elongated in the  $ab$ -plane. When the azimuthal scan is performed around  $c$ -axis, the intensity is almost independent of  $\varphi$ , because the ferro-component of the scattering factor along the  $a$ - and  $b$ -axes is identical under the condition of  $\theta_B^{(t)} = -\theta_A^{(t)}$ .

In Fig. 4(b), the orbital dependence of the intensity at the fundamental reflection with  $\varphi_A = 0$  is shown. With increasing  $\theta_A^{(t)}$  from  $\theta_A^{(t)} = \pi/6$ , the  $\varphi$  dependence becomes weak and is almost smeared out at  $(\theta_A^{(t)}, \theta_B^{(t)}) = (\pi/2, -\pi/2)$ . With further increasing  $\theta_A^{(t)}$ , the phase of the modulation is reversed. In the case of  $\theta_A^{(t)} > \pi/2$ , the ferro-component of the scattering factor in the  $c$ -direction becomes dominant in comparison with that in the  $ab$ -plane. We conclude that through the measurement of the phase of the polarization dependence, we can determine whether  $\theta_A^{(t)}$  is larger or smaller than  $\pi/2$ .

In Fig. 5(a), the orbital superlattice reflection, which appears only in orbital-AF ordering is shown. The orbital state is  $(\theta_A^{(t)}, \theta_B^{(t)}) = (4\pi/6, -4\pi/6)$  which corresponds to  $(3d_{3y^2-r^2}, 3d_{3x^2-r^2})$  ordering. The coordinate in the laboratory system is chosen to be  $(\hat{e}_1, \hat{e}_2, \hat{e}_3) = (\hat{c}, \frac{1}{\sqrt{2}}(\hat{a} - \hat{b}), \frac{1}{\sqrt{2}}(\hat{a} + \hat{b}))$ . The azimuthal scan in this coordinate was carried out in  $\text{La}_{0.5}\text{Sr}_{0.5}\text{MnO}_4$  and  $\text{LaMnO}_3$ .<sup>21,22</sup> The explicit formulae of the polarization dependence at  $\varphi_A = 0$  and  $\pi/2$  are given by

$$\begin{aligned} \tilde{I}(\varphi, \varphi_A = 0) &= |\Delta f_{-zz} \cos^2 \varphi \\ &+ \frac{1}{2}(\Delta f_{-xx} + \Delta f_{-yy}) \sin^2 \varphi|^2, \end{aligned} \quad (26)$$

and

$$\begin{aligned} \tilde{I}(\varphi, \varphi_A = \pi/2) &= \left| \frac{1}{2}(-\Delta f_{-xx} + \Delta f_{-yy}) \sin \varphi \cos \theta \right. \\ &+ \left. \frac{1}{2}(\Delta f_{-xx} + \Delta f_{-yy} - 2\Delta f_{-zz}) \right. \\ &\times \left. \sin \varphi \cos \varphi \sin \theta \right|^2, \end{aligned} \quad (27)$$

respectively. The intensity is expressed only by the antiferro-component of the scattering factor. At this reflection, the information of the orbital ordering is derived without disturbance of the normal part of the scattering factor, in contrast with the case of the fundamental reflection. When the orbital ordering is assumed to

be  $(\theta_A^{(t)}, \theta_B^{(t)} = -\theta_A^{(t)})$ , the condition,  $\Delta f_{Axx} = \Delta f_{Byy}$ ,  $\Delta f_{Ayy} = \Delta f_{Bxx}$  and  $\Delta f_{Azz} = \Delta f_{Bzz}$ , is satisfied. In this case,  $\tilde{I}(\varphi, \varphi_A = 0)$  in Eq.(26) becomes zero, and  $\tilde{I}(\varphi, \varphi_A = \pi/2) = |\frac{1}{2}(\Delta f_{Axx} - \Delta f_{Ayy}) \sin \varphi \cos \theta|^2$  in Eq. (27). These expression gives a square of the sinusoidal symmetry in the polarization dependence as shown in Fig. 5(a). By utilizing this characteristic feature of the polarization dependence, we can judge whether the condition  $(\theta_A^{(t)}, \theta_B^{(t)} = -\theta_A^{(t)})$  is satisfied or not. For example, as shown in Fig. 6, when we assume different types of the orbital-AF ordering  $(\theta_A^{(t)}, \theta_B^{(t)} = \theta_A^{(t)} + \pi)$ , the polarization dependence shows a quite different feature from that in Fig. 5.

In Fig. 5(b), the polarization dependence at  $\varphi_A = \pi/2$  in several orbital-AF cases is presented. Here, the condition  $(\theta_A^{(t)}, \theta_B^{(t)} = -\theta_A^{(t)})$  is assumed. The scattering intensity changes with  $\theta_A^{(t)}$  and becomes maximum around  $\theta_A^{(t)} = \pi/2$ . The polarization dependence is, however, given by a square of the sinusoidal function in all cases. In the azimuthal analyses performed in  $\text{La}_{0.5}\text{Sr}_{1.5}\text{MnO}_4$ <sup>21</sup>, the experimental data are well fitted by the above function. Therefore, we conclude that the orbital ordering in  $\text{La}_{0.5}\text{Sr}_{1.5}\text{MnO}_4$  satisfies the condition  $(\theta_A^{(t)}, \theta_B^{(t)} = -\theta_A^{(t)})$ , i.e., the  $A$  and  $B$  orbitals are symmetric with respect to replacement of  $x(y)$  by  $y(x)$ . However, we can not determine which type of the orbital ordering,  $(3d_{3x^2-r^2}, 3d_{3y^2-r^2})$  or  $(3d_{z^2-x^2}, 3d_{y^2-z^2})$  is realized, through the measurement of this reflection.

### C. orbital ordering in charge ordered state

The charge ordering,<sup>15,16,21</sup> where  $\text{Mn}^{3+}$  and  $\text{Mn}^{4+}$  ions are alternately aligned in the  $\text{MnO}_2$  plane, have been observed in  $\text{R}_{1-x}\text{A}_x\text{MnO}_3$  near  $x = 0.5$  and  $\text{La}_{0.5}\text{Sr}_{1.5}\text{MnO}_4$ .<sup>15,16,21</sup> In the latter compound, it is accompanied with the orbital ordering<sup>21</sup> and the CE-type spin ordering. In this subsection, we investigate the polarization dependence of the scattering intensity in the charge ordered phase and propose the possibility to identify the orbital ordering in this phase.

We consider the alternating alignment of  $\text{Mn}^{3+}$  and  $\text{Mn}^{4+}$  ions in the  $\text{MnO}_2$  plane and introduce two kinds of the orbital sublattice for  $\text{Mn}^{3+}$  ion, denoted by  $A$  and  $B$ . It is assumed that a  $\text{Mn}^{3+}$  ion has  $A(B)$  orbital, when the spin in a  $\text{Mn}^{3+}$  ion is parallel to that in its neighboring  $\text{Mn}^{4+}$  ions in the  $a(b)$ -direction.<sup>5,6,12,15,21</sup> This type of orbital ordering is consistent with the CE-type spin structure. Here, we pay our attention to the reflection at  $(h k l) = (n_x + \frac{1}{2} n_y + \frac{1}{2} n_z)$  termed the charge-order reflection, which appears due to the existence of the charge ordering. The structure factor at the reflection is given by

$$F_{\alpha\beta} = N(\tilde{f}_{A\alpha\beta} + \tilde{f}_{B\alpha\beta} - 2f_{4\alpha\beta}), \quad (28)$$

where  $\tilde{f}_{A(B)\alpha\beta}$  is the scattering factor defined in the orthohombic coordinate as follows

$$\tilde{f}_{l\alpha\beta} = \begin{pmatrix} \frac{1}{2}(f_{lxx} + f_{lyy}) & \frac{1}{2}(f_{lxx} - f_{lyy}) & 0 \\ \frac{1}{2}(f_{lxx} - f_{lyy}) & \frac{1}{2}(f_{lxx} + f_{lyy}) & 0 \\ 0 & 0 & f_{lzz} \end{pmatrix}, \quad (29)$$

for  $l = A$  and  $B$ .  $f_4$  is the atomic scattering factor of  $\text{Mn}^{4+}$  ions. We emphasize that the difference of the normal part of the scattering factor  $f_{0A} + f_{0B} - 2f_{04}$  is of the order of (one electron)/(Mn atom), which is much smaller than the typical value of the anomalous part at the edge. Furthermore, the anomalous part of the scattering factor of a  $\text{Mn}^{4+}$  ion is scalar. Its value is smaller than that of  $\text{Mn}^{3+}$  ions near the K-edge of a  $\text{Mn}^{3+}$  ion, because the edge is lower than that of a  $\text{Mn}^{4+}$  ion.<sup>21</sup> Therefore, by utilizing this reflection, we can obtain the information of the ferro-component of the scattering factor without disturbance of the normal part.

In Fig. 7(a), the polarization dependence of the scattering intensity at the charge-order reflection is presented. The types of the orbital is  $(\theta_A^{(t)}, \theta_B^{(t)}) = (4\pi/6, -4\pi/6)$ . The coordinate in the laboratory system is chosen to be  $(\hat{e}_1, \hat{e}_2, \hat{e}_3) = (\hat{c}, \frac{1}{\sqrt{2}}(\hat{a} - \hat{b}), \frac{1}{\sqrt{2}}(\hat{a} + \hat{b}))$ . We neglect the contribution from  $f_{0A} + f_{0B} - 2f_{04}$ , and assume that the anomalous part of the scattering factor in a  $\text{Mn}^{4+}$  ion as a scalar, that is,  $\Delta f_{4\alpha\beta} = \Delta f_4 \delta_{\alpha\beta}$ , and the value of  $\Delta f_4$  is a half of the maximum value of  $|\Delta f_{l\alpha\alpha}|$  ( $l = A, B$ ) ( $\alpha = x, y, z$ ) in a  $\text{Mn}^{3+}$  ion.<sup>21</sup> The explicit formula at  $\varphi_A = 0$  is given by

$$\begin{aligned} \tilde{I}(\varphi, \varphi_A = 0) = & \frac{1}{16} |(\Delta f_{+xx} + \Delta f_{+yy}) \sin^2 \varphi \\ & + 2\Delta f_{+zz} \cos^2 \varphi - 2\Delta f_4|^2. \end{aligned} \quad (30)$$

In the case of  $\varphi = 0$  and  $\pi$  in Fig. 7(a), the electric vector in the incident beam is parallel to the  $c$ -axis. It is worth noting that the polarization dependence in Fig. 7(a) is more remarkable in contrast with that shown in Fig. 4(a), because the scalar component of the scattering factor is smaller in the present case. Furthermore, the intensity in the case where the electric vector is parallel to the  $ab$ -plane becomes maximum, that is, the polarization dependence is opposite to the case in Fig. 4(a). This is attributed to the fact that the polarization dependence is dominated by the anomalous term of  $\text{Mn}^{3+}$  ions. On the other hand, in Fig. 4(a) the interference term between the normal and anomalous parts determines the polarization dependence. As shown in Fig. 7(b), the phase of the polarization dependence for  $\theta_A^{(t)} > \pi/2$  is opposite to that for  $\theta_A^{(t)} < \pi/2$ . It is concluded that in the charge ordered state, by utilizing the polarization dependence of the charge-order reflection the ferro-component of the scattering factor in orbital-AF state is identified easier than in the case of fundamental reflection.

## V. SUMMARY AND DISCUSSION

In this paper, we have theoretically investigated the anomalous X-ray scattering as a probe to detect the orbital ordering in manganites. Through the polarization dependence of the scattering factor, we showed how to identify several types of the orbital ordering. In particular, we paid our attention to the method to distinguish the two types of the orbital orderings;  $(3d_{3x^2-r^2}, 3d_{3y^2-r^2})$  or  $(3d_{z^2-x^2}, 3d_{y^2-z^2})$ .

At the superlattice reflection due to the antiferro-type orbital ordering with the condition  $\theta_B^{(t)} = -\theta_A^{(t)}$ , the azimuthal angle dependence is represented by a square of the sinusoidal function and its intensity depends on types of orbital (Fig. 5). We found that it is difficult to determine which orbital ordering  $(3d_{3x^2-r^2}, 3d_{3y^2-r^2})$  or  $(3d_{z^2-x^2}, 3d_{y^2-z^2})$  is realized by analyzing the results at the reflection. This difficulty is attributed to the fact that the antiferro-component  $\frac{1}{2}(\Delta f_{A\alpha\beta} - \Delta f_{B\alpha\beta})$  of the scattering factor is observed at the superlattice reflection. Then, we have proposed two kinds of polarization analyses where the ferro-component of the scattering factor, i.e.,  $\frac{1}{2}(\Delta f_{A\alpha\beta} + \Delta f_{B\alpha\beta})$ , is derived.

The first one is the polarization analyses at the fundamental reflection (Fig. 4), where the scattering factor is represented by sum of the normal part and the ferro-component of the anomalous part. The interference between them gives rise to the polarization dependence of the scattering intensity. Since the normal part is much larger than the anomalous one, the orbital ordering reflects on the modulation in the polarization dependence. In order to detect the modulation, the reflection plane is required not to include the heavy ions, such as a La ion, because the large values of the normal part disturbs to detect the modulation. The reflection with the large scattering angle characterized by the large number of  $(hkl)$  is also suitable, because the normal part of the scattering factor is reduced with increasing the scattering momentum, in contrast with the anomalous part.

The second proposal to obtain the ferro-component of the scattering factor is the analyses at charge-order reflection points in charge ordered phases (Fig. 7). At the reflection, the normal part is almost canceled out. The scattering factor is dominated by the ferro-component of the anomalous scattering factor in a  $\text{Mn}^{3+}$  ion and the anomalous part in a  $\text{Mn}^{4+}$  ion. The latter is a scalar and its value is smaller than that of a  $\text{Mn}^{3+}$  ion near the  $\text{Mn}^{3+}$  K-edge. Therefore, by analyzing the polarization dependence of this reflection, the ferro-component of the scattering factor is observed. It is noted that the basic considerations in the above theoretical proposals are independent of details in the numerical microscopic calculation and are based on symmetry of types of the orbital ordering and the experimental arrangement.

In conclusion, we have shown that in the anomalous X-ray scattering technique, types of the orbital order is able to be identified by selecting the adequate reflection

point and analyzing the polarization dependence of the scattering intensity.

## ACKNOWLEDGMENTS

We would like to thank Y. Endoh and Y. Murakami for providing the experimental data prior to publication and for valuable discussions. We also indebted to W. Koshiba for helpful comments. This work was supported by Priority Areas Grants from the Ministry of Education, Science and Culture of Japan, and CREST (Core Research for Evolutional Science and Technology Corporation) Japan. Part of the numerical calculation was performed in the HITACS-3800/380 supercomputing facilities in Institute for Materials Research, Tohoku University.

---

<sup>1</sup> K. Chahara, T. Ohono, M. Kasai, Y. Kanke, and Y. Kozono, *Appl. Phys. Lett.* **62**, 780 (1993).

<sup>2</sup> R. von Helmolt, J. Wecker, B. Holzapfel, L. Schultz, and K. Samwer, *Phys. Rev. Lett.* **71**, 2331 (1993).

<sup>3</sup> Y. Tokura, A. Urushibara, Y. Moritomo, T. Arima, A. Asamitsu, G. Kido, and N. Furukawa, *J. Phys. Soc. Jpn.* **63**, 3931 (1994).

<sup>4</sup> S. Jin, T. H. Tiefel, M. McCormack, R. A. Fastnacht, R. Ramesh, and L. H. Chen, *Science*, **264**, 413 (1994)

<sup>5</sup> J. B. Goodenough, *Phys. Rev.* **100**, 564 (1955).

<sup>6</sup> J. Kanamori, *J. Phys. Chem. Solids*, **10**, 87 (1959).

<sup>7</sup> K. I. Kugel and D. I. Khomskii, *JETP Lett.* **15**, 446 (1972).

<sup>8</sup> N. Hamada, H. Sawada, and K. Terakura, in *Spectroscopy of Mott insulators and correlated metals*, Solid State Sciences 119, (Springer-Verlag, Berlin), (1995).

<sup>9</sup> T. Mizokawa, and A. Fujimori, *Phys. Rev. B* **51**, 12880 (1995).

<sup>10</sup> S. Ishihara, J. Inoue, and S. Maekawa, *Physica C* **263**, 130 (1996), and *Phys. Rev. B* **55**, 8280 (1997).

<sup>11</sup> S. Ishihara, M. Yamanaka, and N. Nagaosa, *Phys. Rev. B* **56**, 686 (1997).

<sup>12</sup> E. O. Wollan, and W. C. Koehler, *Phys. Rev.* **100**, 545 (1955).

<sup>13</sup> G. Matsumoto, *J. Phys. Soc. Jpn.* **29**, 606 (1970).

<sup>14</sup> Z. Jirak, S. Krupicka, Z. Simsa, M. Dlouha, and S. Vratislav, *J. Mag. Mag. Mat.* **53**, 153 (1985).

<sup>15</sup> C. H. Chen, and S.-W. Cheong, *Phys. Rev. Lett.* **76**, 4042 (1996), P. G. Radaeli, D. E. Cox, M. Marezio, and S.-W. Cheong, *Phys. Rev. B* **55**, 3015 (1997).

<sup>16</sup> B. J. Sternlieb, J. P. Hill, U. C. Wildgruber, G. M. Luke, C. B. Nachumi, Y. Moritomo, and Y. Tokura, *Phys. Rev. Lett.* **76**, 2169 (1996).

<sup>17</sup> R. Maezono, S. Ishihara, and N. Nagaosa, *Phys. Rev. B* **57**, R13993 (1998).

<sup>18</sup> M. Imada, *J. Phys. Soc. Jpn.* **67**, 45 (1998).

<sup>19</sup> H. Shiba, R. Shiina, and A. Takahashi, *J. Phys. Soc. Jpn.* **66**, 941 (1997).

<sup>20</sup> Y. Ito, and J. Akimitsu, *J. Phys. Soc. Jpn.* **40**, 1333 (1976).

<sup>21</sup> Y. Murakami, H. Kawada, H. Kawata, M. Tanaka, T. Arima, H. Moritomo and Y. Tokura, *Phys. Rev. Lett.* **80**, 1932 (1998).

<sup>22</sup> Y. Murakami, J. P. Hill, D. Gibbs, M. Blume, I. Koyama, M. Tanaka, H. Kawata, T. Arima, T. Tokura, K. Hirota, and Y. Endoh, *Phys. Rev. Lett.* **81**, 582 (1998).

<sup>23</sup> Y. Endoh, K. Hirota, Y. Murakami, T. Fukuda, H. Kimura, N. Nojiri, K. Kaneko, S. Ishihara, S. Okamoto, and S. Maekawa, (unpublished).

<sup>24</sup> S. Ishihara, S. Okamoto, and S. Maekawa, *J. Phys. Soc. Jpn.* **66**, 2965 (1997).

<sup>25</sup> W. Koshiba, Y. Kawamura, S. Ishihara, S. Okamoto, J. Inoue, and S. Maekawa, *J. Phys. Soc. Jpn.* **66**, 957 (1997).

<sup>26</sup> W. Koshiba, Y. Kawamura, J. Inoue, and S. Maekawa, *J. Phys. Soc. Jpn.* **66**, 2985 (1997).

<sup>27</sup> R. Shiina, T. Nishitani and H. Shiba, *J. Phys. Soc. Jpn.* **66**, 3159 (1997).

<sup>28</sup> T. Mizokawa, and A. Fujimori, *Phys. Rev. B* **56**, R493 (1997).

<sup>29</sup> D. H. Templeton, and L. K. Templeton, *Acta Cryst.* **A38**, 62 (1982), *ibid.* **A41**, 133 (1985).

<sup>30</sup> V. E. Dmitrienko, *Acta Cryst.* **A39**, 29 (1983).

<sup>31</sup> S. Ishihara, and S. Maekawa, *Phys. Rev. Lett.* **80**, 3799 (1998).

<sup>32</sup> E. Tsuji, T. Kurasawa, I. Yazawa, H. Katoh, N. Nomozawa, K. Ishida, and S. Kishimoto, *J. Phys. Soc. Jpn.* **65**, 610 (1996), T. Nagano, J. Kokubun, I. Yazawa, T. Kurasawa, M. Kurabayashi, E. Tsuji, K. Ishida, S. Sasaki, T. Mori, S. Kishimoto, and Y. Murakami, *J. Phys. Soc. Jpn.* **65**, 3060 (1996).

<sup>33</sup> A. Kirsch, and A. Petcov, *Acta Cryst. A* **47**, 180 (1991).

<sup>34</sup> A. V. Kolpakov, V. A. Bushuev, and R. N. Kuz'min, *Sov. Phys. Usp.* **21**, 959 (1978).

<sup>35</sup> M. Blume, in *Resonant Anomalous X-ray Scattering- Theory and Applications* edited by G. Materlik, C.J. Sparks, and K. Fischer. Elsevier Science B.V. (1994).

<sup>36</sup> M. Fabrizio, M. Altarelli, and M. Benfatto, *Phys. Rev. Lett.* **80**, 3400 (1998).

<sup>37</sup> H. Kawano, R. Kajimoto, M. Kubota, and H. Yoshizawa, *Phys. Rev. B* **53**, R14709 (1996).

<sup>38</sup> Y. Murakami (private communication).

<sup>39</sup> T. Saitoh, A. E. Bocquet, T. Mizokawa, H. Namatame, A. Fujimori, M. Abbate, T. Takeda, and M. Takano, *Phys. Rev. B* **51**, 13942 (1995).

Figure captions.

Fig. 1: The schematic view of the experimental arrangement<sup>21,32</sup> which consists of a sample crystal ( $S$ ), analyzer crystal ( $A$ ) and photon detector ( $D$ ). The polarization dependence of the scattering intensity is measured as a function of the azimuthal angle ( $\varphi$ ) and the analyzer angle ( $\varphi_A$ ).  $\vec{k}'$  ( $\vec{k}''$ ) is the photon momentum and  $\pi'$  ( $\pi''$ ) and  $\sigma'$  ( $\sigma''$ ) are the polarization of the incident(scattered) photon.

Fig. 2: The real and imaginary parts of the scattering factor ( $(\Delta f_i)_{xx(yy,zz)} m/|A|^2$ ) in the cases where the following orbitals are occupied: (a), (b)  $\theta^{(t)} = 0$  ( $3d_{3z^2-r^2}$ ), and (c), (d)  $\theta^{(t)} = \pi$  ( $3d_{x^2-y^2}$ ). The straight and broken lines show  $(\Delta f_i)_{xx(yy)}$  and  $(\Delta f_i)_{zz}$ , respectively. The parameter value of  $\delta$  in Eq.(14) is chosen to be 0.5eV. The origin of the energy is taken to be arbitrary. The spectra of  $(\Delta f_i)_{xx}$  and  $(\Delta f_i)_{yy}$  are identical.

Fig. 3: The polarization dependence of the scattering intensity in the orbital-F case. The coordinate in the laboratory system is chosen to be  $(\hat{e}_1, \hat{e}_2, \hat{e}_3) = (\hat{b}, \hat{c}, \hat{a})$ , where  $(\hat{a}, \hat{b}, \hat{c})$  represents the cubic crystallographic coordinate. (a): The orbital is chosen to be  $\theta_A^{(t)} = 0$  ( $3d_{3z^2-r^2}$ ). (b) : The azimuthal angle dependence at  $\varphi_A = 0$  in several orbital-F cases.

Fig. 4: The polarization dependence of the scattering intensity of the fundamental reflection in the orbital-AF case. The coordinate in the laboratory system is chosen to be  $(\hat{e}_1, \hat{e}_2, \hat{e}_3) = (\hat{b}, \hat{c}, \hat{a})$  where  $(\hat{a}, \hat{b}, \hat{c})$  represents the cubic crystallographic coordinate. (a) :  $(\theta_A^{(t)} = 4\pi/6, \theta_B^{(t)} = -4\pi/6)$  orbital ( $(3d_{3y^2-r^2}, 3d_{3x^2-r^2})$ ) is assumed. (b): The azimuthal angle dependence at  $\varphi_A = 0$  in several orbital-AF cases with  $(\theta_A^{(t)}, \theta_B^{(t)} = -\theta_A^{(t)})$ .

Fig. 5: The polarization dependence of the scattering intensity of the orbital superlattice reflection in the orbital-AF case. The coordinate in the laboratory system is chosen to be  $(\hat{e}_1, \hat{e}_2, \hat{e}_3) = (\hat{c}, \frac{1}{\sqrt{2}}(\hat{a} - \hat{b}), \frac{1}{\sqrt{2}}(\hat{a} + \hat{b}))$ , where  $(\hat{a}, \hat{b}, \hat{c})$  represents the cubic crystallographic coordinate. (a):  $(\theta_A^{(t)} = 4\pi/6, \theta_B^{(t)} = -4\pi/6)$  orbital ( $(3d_{3y^2-r^2}, 3d_{3x^2-r^2})$ ) is assumed. (b) : The azimuthal angle dependence at  $\varphi_A = \pi/2$  in several orbital-AF cases with  $(\theta_A^{(t)}, \theta_B^{(t)} = -\theta_A^{(t)})$ .

Fig. 6: The polarization dependence of the scattering intensity of the orbital superlattice reflection in the orbital-AF case. The coordinate in the laboratory system is chosen to be  $(\hat{e}_1, \hat{e}_2, \hat{e}_3) = (\hat{c}, \frac{1}{\sqrt{2}}(\hat{a} - \hat{b}), \frac{1}{\sqrt{2}}(\hat{a} + \hat{b}))$ , where  $(\hat{a}, \hat{b}, \hat{c})$  represents the cubic crystallographic coordinate. (a):  $(\theta_A^{(t)} = 0, \theta_B^{(t)} = \pi)$  orbital ( $(3d_{3z^2-r^2}, 3d_{x^2-y^2})$ ) is assumed. (b) : The azimuthal angle dependence at  $\varphi_A = \pi/2$  in several orbital-AF cases with  $(\theta_A^{(t)}, \theta_B^{(t)} = \theta_A^{(t)} + \pi)$ .

Fig. 7: The polarization dependence of the scattering intensity at the  $(n_x + \frac{1}{2}n_y + \frac{1}{2}n_z)$  reflection (charge-order reflection). The coordinate in the laboratory system is chosen to be  $(\hat{e}_1, \hat{e}_2, \hat{e}_3) = (\hat{c}, \frac{1}{\sqrt{2}}(\hat{a} - \hat{b}), \frac{1}{\sqrt{2}}(\hat{a} + \hat{b}))$  where  $(\hat{a}, \hat{b}, \hat{c})$  represents the cubic crystallographic coordinate. (a):  $(\theta_A^{(t)} = 4\pi/6, \theta_B^{(t)} = -4\pi/6)$  orbital ( $(3d_{3y^2-r^2}, 3d_{3x^2-r^2})$ ) is as-

sumed. (b) : The azimuthal angle dependence at  $\varphi_A = 0$  in several orbital-AF cases with  $(\theta_A^{(t)}, \theta_B^{(t)} = -\theta_A^{(t)})$ .

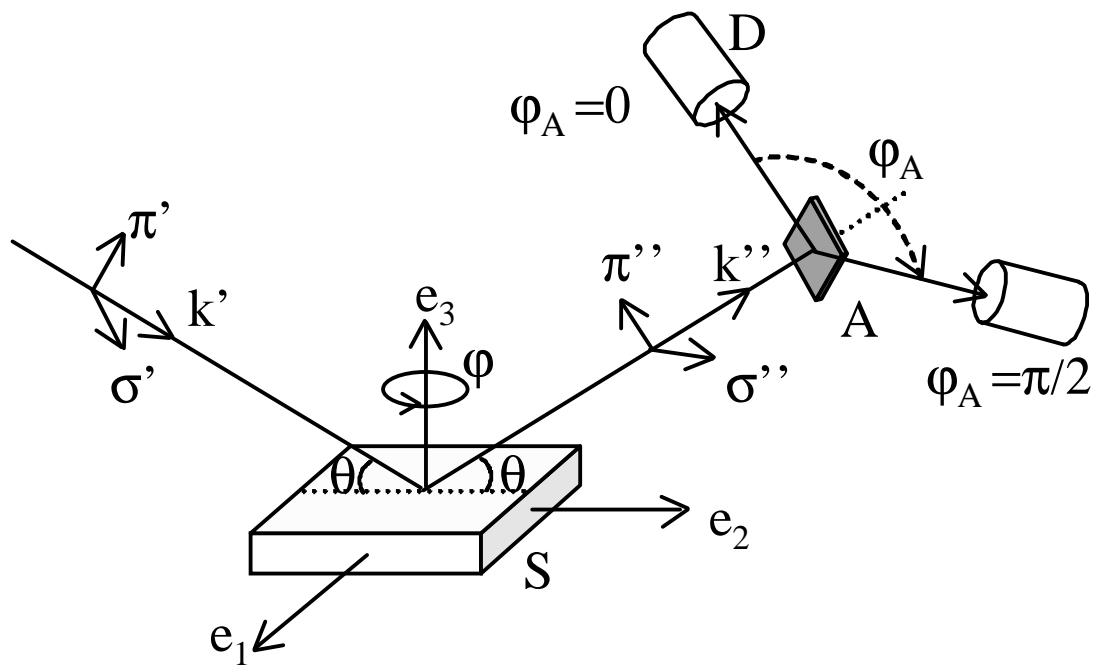


Fig. 1 S.Ishihara et al.

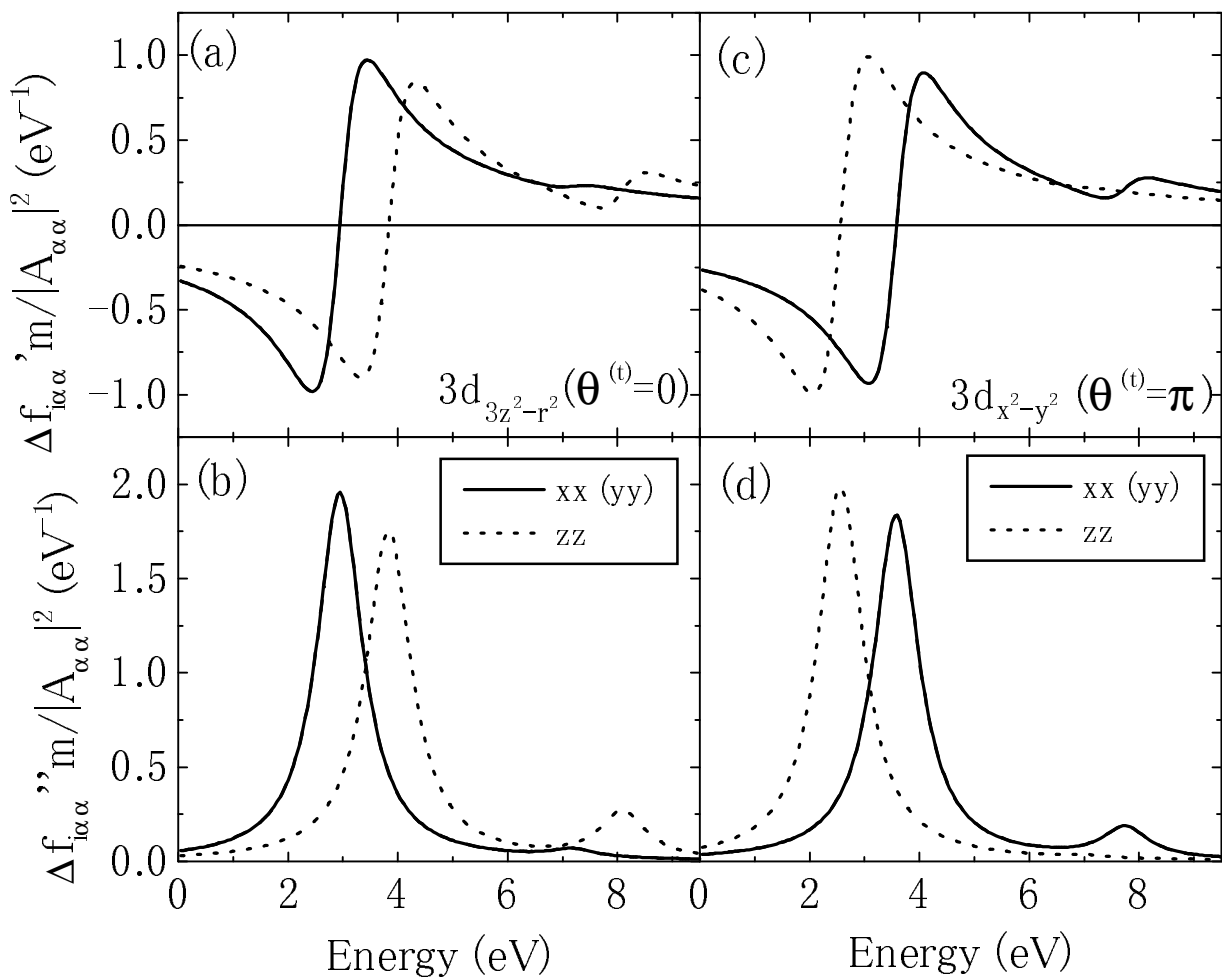
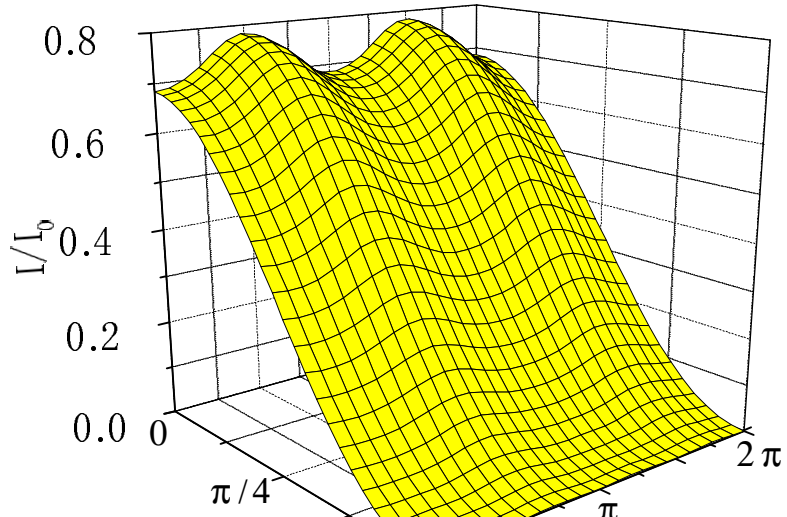


Fig. 2 S.Ishihara et al.

(a)  $\theta_A^{(t)}=0$  (3d  $3z^2-r^2$ )



(b)

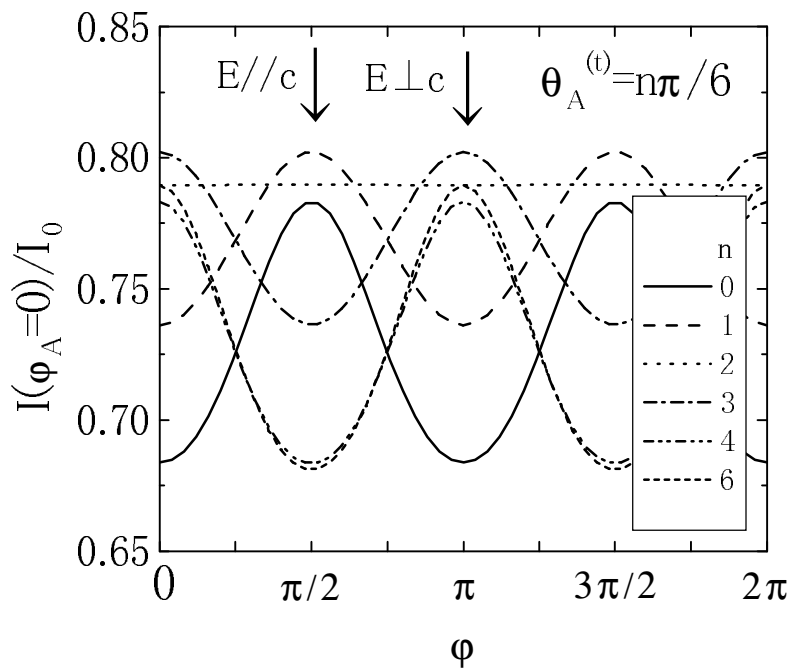
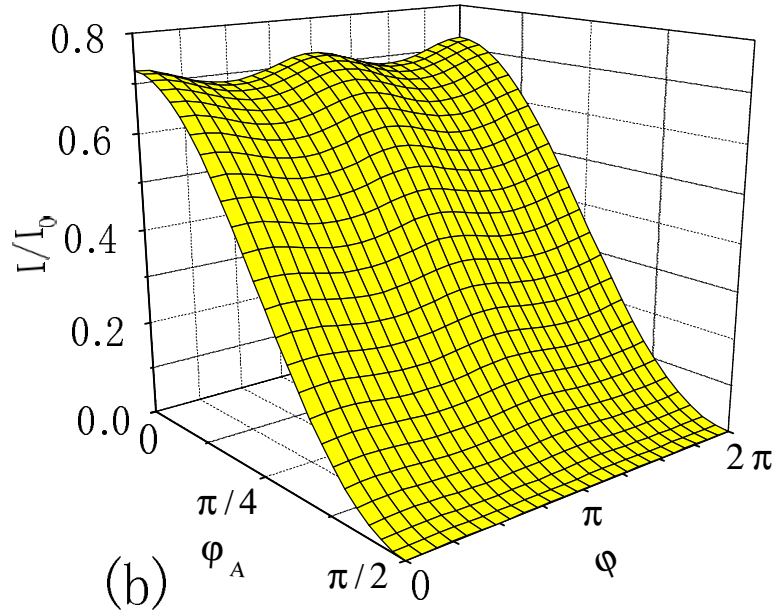


Fig. 3 S.Ishihara et al.

(a)  $\theta_A^{(t)} = 4\pi/6$  ( $3d_{3y^2-r^2}$ ,  $3d_{3x^2-r^2}$ )



(b)

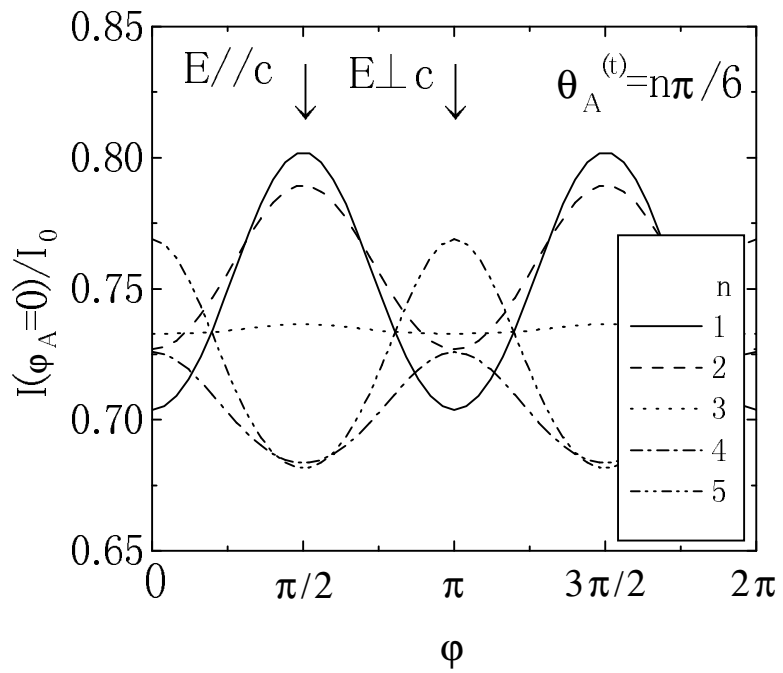
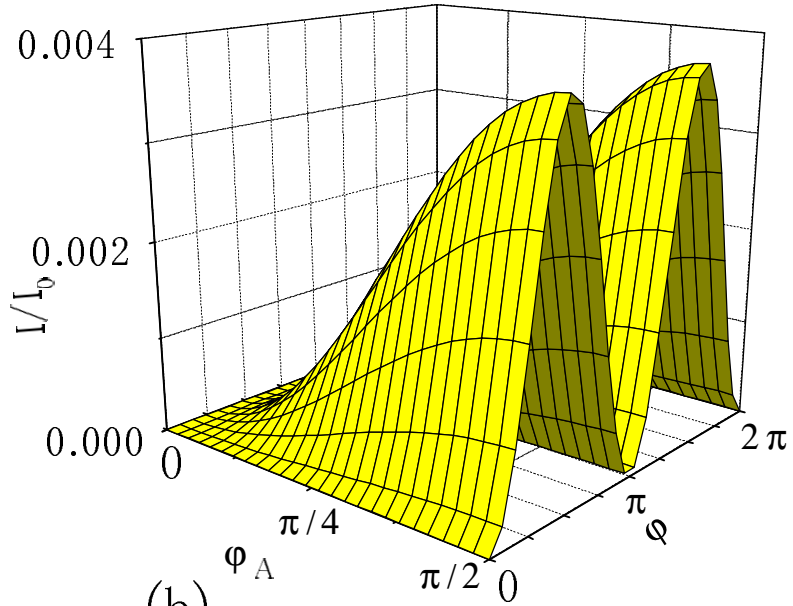


Fig. 4 S.Ishihara et al.

(a)  $\theta_A^{(t)} = 4\pi/6 (3d_{3y^2-r^2}, 3d_{3x^2-r^2})$



(b)

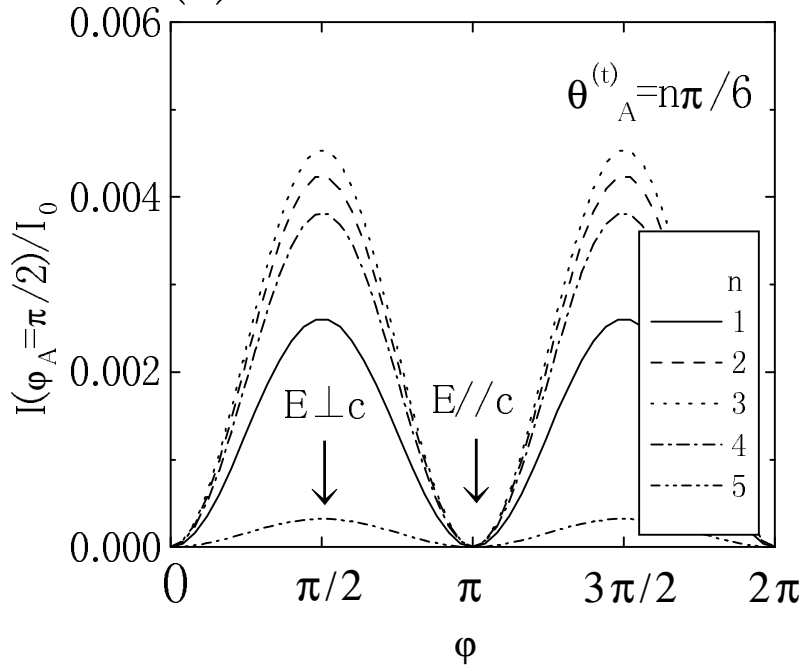
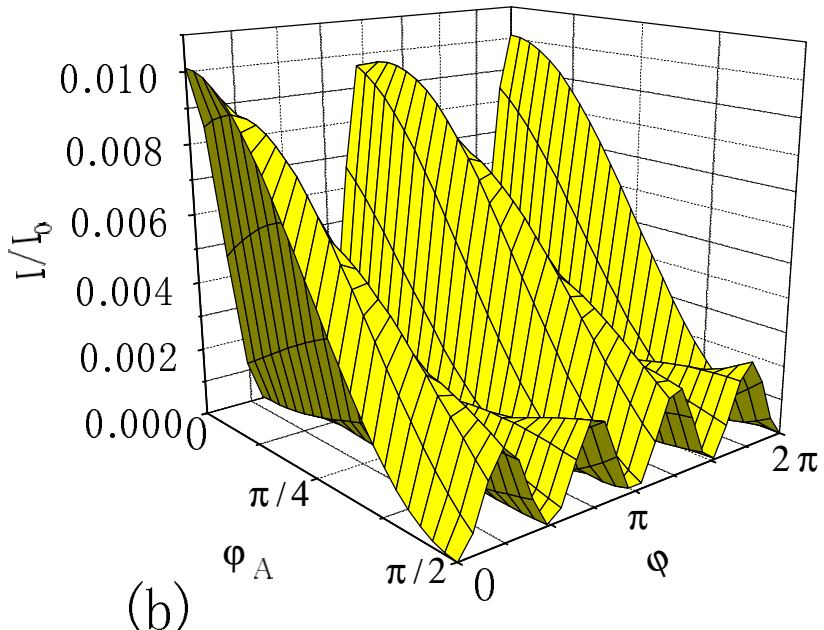


Fig. 5 S.Ishihara et al.

(a)  $\theta_A^{(t)} = 0$   $(3d_{3z^2-r^2}, 3d_{x^2-y^2})$



(b)

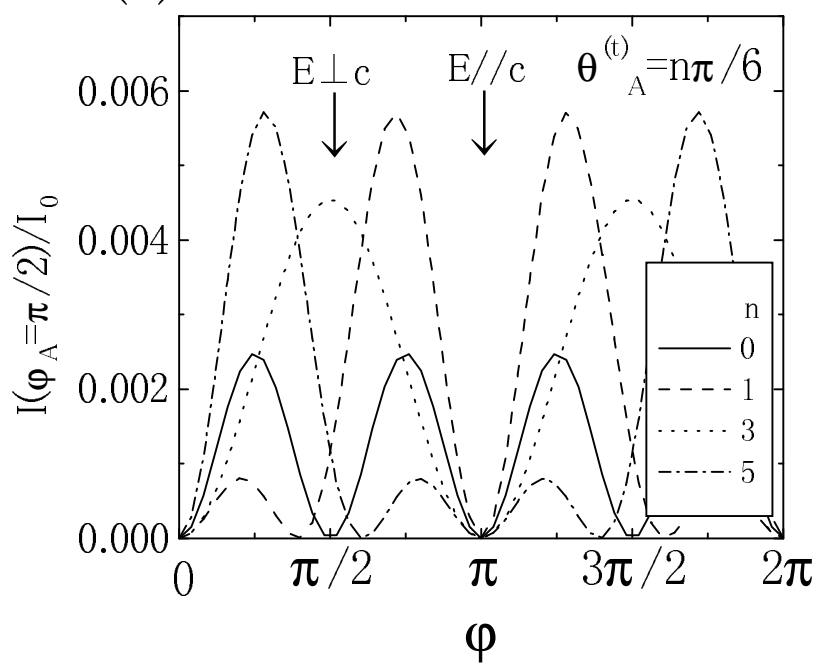
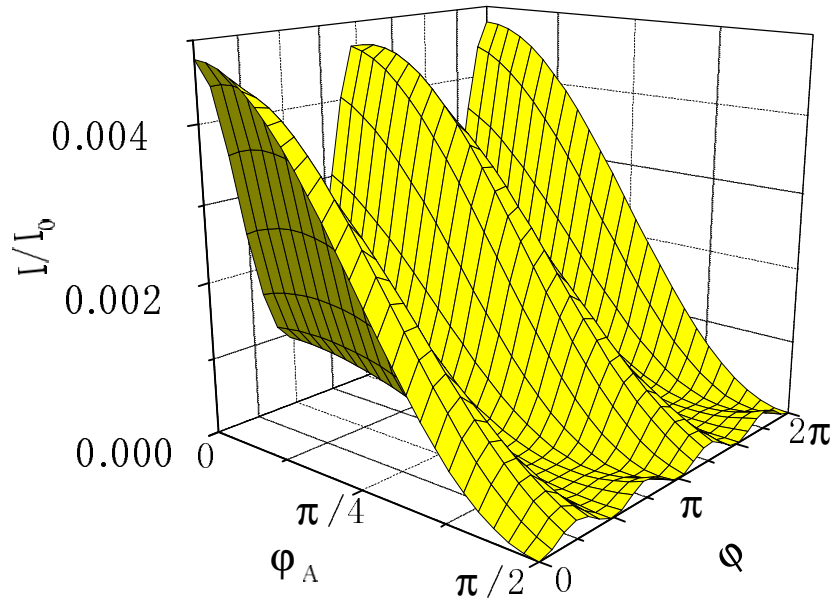


Fig. 6 S.Ishihara et al.

(a)  $\theta_A^{(t)} = 4\pi/6$        $(3d_{3y^2-r^2}, 3d_{3x^2-r^2})$



(b)

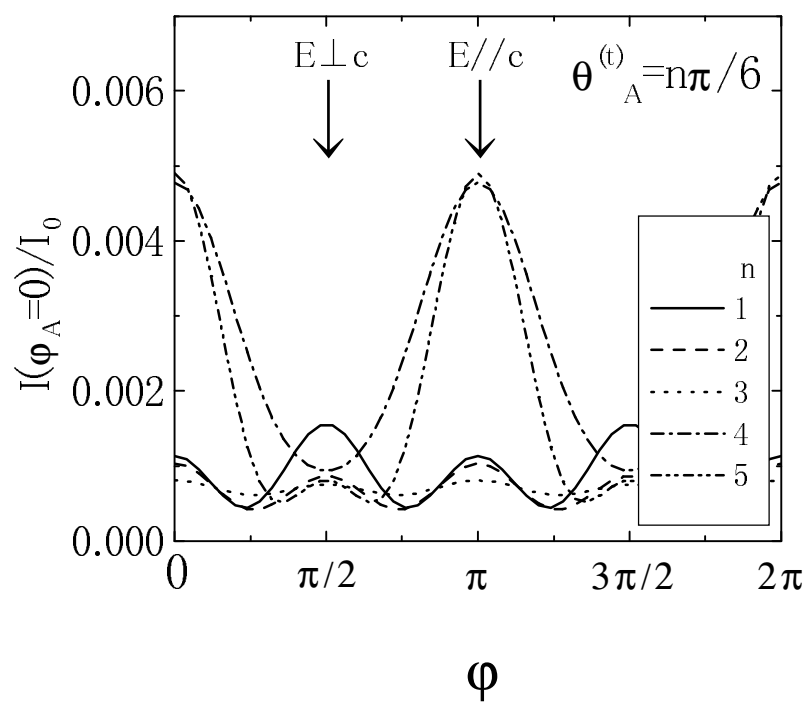


Fig. 7 S.Ishihara et al.